2022

Thermal-Fluid Performance Modelling Of A Transcritical Carbon Dioxide Heat Pump For High Temperature Applications

Martin van Eldik

Philip van Zyl Venter

Michael Botha

Thermal-Fluid Performance Modelling Of A Transcritical Carbon Dioxide Heat Pump For High Temperature Applications

Martin VAN ELDIK[1]*, Philip VENTER[2], Michael BOTHA[3]

North-West University, School of Mechanical Engineering,
Potchefstroom, South Africa
[1]+27(0)182994283, martin.vaneldik@nwu.ac.za
[2]philip.venter@nwu.ac.za
[3]michael.botha@gmail.com

* Corresponding Author

ABSTRACT

The South African industrial sector is mainly dependent on the use of electricity and coal for the generation of process heat. The environmental impact of the existing methods is such that implementing alternative heating solutions are unavoidable. One solution, to reduce electrical consumption, is the implementation of energy efficient air-to-water heat pumps in place of existing technologies for the lower range of process temperature requirements of up to 100°C. Conventional heat pumps, however, have a limitation to generate warm water efficiently above about 65°C. Furthermore, the negative environmental impact of freon based systems encourages the need to consider the implementation of natural refrigerants. Carbon dioxide (R744) has been identified as a working fluid due to the low environmental impact and the capability to deliver higher discharge water temperatures while maintaining a high efficiency. To achieve this the CO_2 heat pump cycle needs to be operated transcritical with very high system pressures. Research has focused on the detailed modelling of the individual components, but the next step is to develop a complete heat pump cycle simulation model. This paper discusses the simulation model developed, and preliminary results obtained, when operating in warm South African ambient conditions, while heating water to temperatures required for industrial processes.

1. INTRODUCTION

According to the 2021 World Energy Outlook report, the industrial sector contributes about 40% of the global energy consumption (IEA, 2021). The South African industrial sector is mainly dependent on the use of electricity and coal for the generation of process heat. A solution to reduce the electrical consumption is the use of energy efficient air-to-water heat pumps for process temperatures below 100°C. Carbon dioxide (R744) as refrigerant is being investigated due to a low environmental impact and the capability to deliver high discharge water temperatures while maintaining a good efficiency. To achieve this the cycle needs to be operated transcritical at very high pressures. R744 has evolved into the leading refrigerant of choice for a multitude of refrigeration and heat pump applications (Cao, et al., 2020). Unfortunately, performance data of the technology for industrial process applications are limited. especially in cases where the system is operated at ambient conditions exceeding 25°C, typical of South African daytime weather.

In literature most studies on R744 include water delivery temperatures of roughly 65°C and ambient temperature ranging from -15°C to 25°C. Three studies reported on the cycle performance at water delivery temperatures of 90°C or higher (Cao, et al., 2020; Yamaguchi, et al., 2011; Ye, et al., 2020), for air-source heat pumps with the highest ambient temperature investigated being 28°C. For a water inlet temperature of 20°C, when the ambient temperature was increased from 13°C to 28°C, the heating COP increased from 3.2 to 3.8, with the heating capacity increasing from 20.8 kW to 27 kW (Yamaguchi *et al.*, 2011). The accompanying discharge pressure remained relatively constant at around 12.5 MPa, as the evaporation temperature rose from 4.3°C to 14.0°C. Cao et al. (2020) found that when the water outlet temperature is raised from 70°C to 90°C, an increase in R744 discharge pressure from 9.8 MPa to 11.9 MPa is experienced with a change in heating capacity from 53.8 kW to 55.8 kW. This was for an ambient temperature of 2°C and a water inlet temperature of 10°C. An 8.3% decrease in the system COP_H from 3.00 to 2.75 was found. Over an ambient temperature range of -10°C to 20°C, Ye *et al.* (2020) recorded a rise in

R744 discharge pressure from 10.2 MPa to 12.7 MPa when heating water from 15°C to 90°C. It was reported that the effect of ambient temperature on the R744 discharge pressure lessens with an increase in water inlet temperature. Over the last decade, research at the North-West University, South Africa, has focused on the detailed modelling of the individual components of the heat pump cycle operated in a transcritical region, with validation using a fully instrumented test bench. The current phase of research focuses on the development of a detailed cycle simulation model, to be discussed in this paper, with the aim to determine system performance in warm ambient conditions typically between 25°C and 40°C experienced in South Africa, while heating water to 90°C as required for industrial processes.

2. HEAT EXCHANGERS MODELLING APPROACH

This section focuses on the modelling approach and correlations used to describe the heat exchangers of the transcritical R744 heat pump cycle shown schematically in Figure 1. The figure also shows the numbering convention used in the modelling approach. The heat exchangers consist of a tube-in-tube refrigerant-to-water gas cooler, and a finned coil air-to-refrigerant evaporator. The semi-hermetic reciprocating compressor selected for the simulations will be discussed in Section 3 along with the other system design specifications.

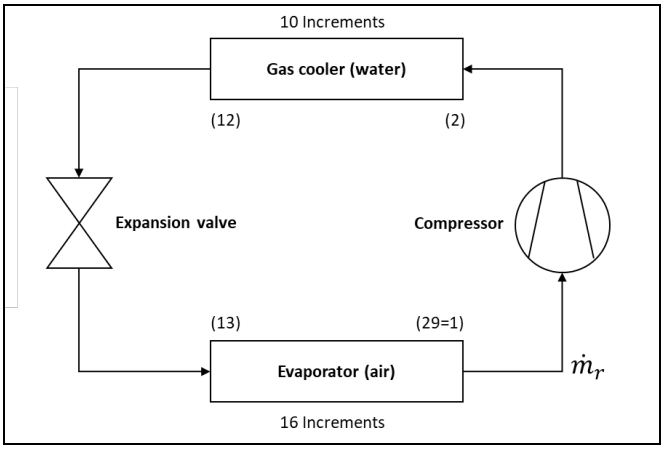

Figure 1: Schematic of an air-to-water transcritical heat pump cycle.

2.1 Gas cooler

Figure 2 is a schematic of the counterflow tube-in-tube gas cooler, where the R744 flows through the inner tube and the water through the annulus. To achieve high discharge water temperatures the R744 in the gas cooler is super-critical. For the modelling of the gas cooler, the finite control volume method is used by discretizing into equal-length increments along the flow path (Kim *et al.*, 2005).

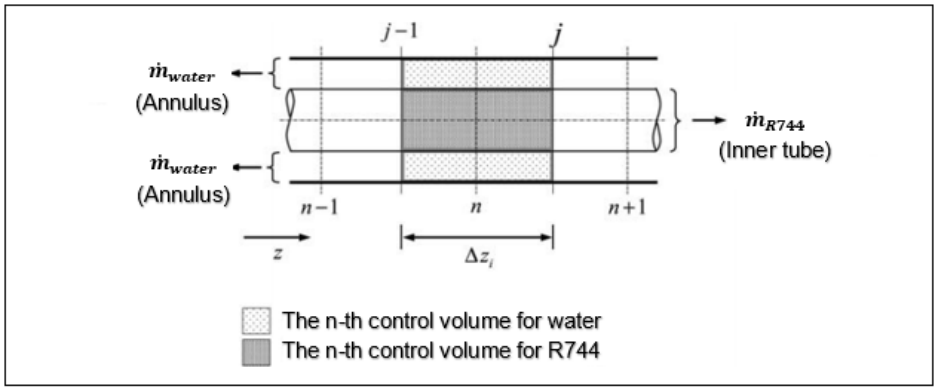

Figure 2: A tube-in-tube gas cooler increment (Kim *et al.*, 2005).

The conservation of mass, momentum and energy are applied to each increment along with the relevant component characteristics such as the heat transfer and pressure drop correlations for both fluids. Geometrical inputs to the model include the diameters and materials for both tubes and the total length of the gas cooler. The boundary conditions used include the compressor outlet temperature and pressure, water inlet temperature and pressure, and the mass flow rates of both fluids. The flow diagram in Figure 3 represents the gas cooler modelling approach followed, with the R744 inlet and outlet states corresponds with points (2) and (12) as denoted in Figure 1.

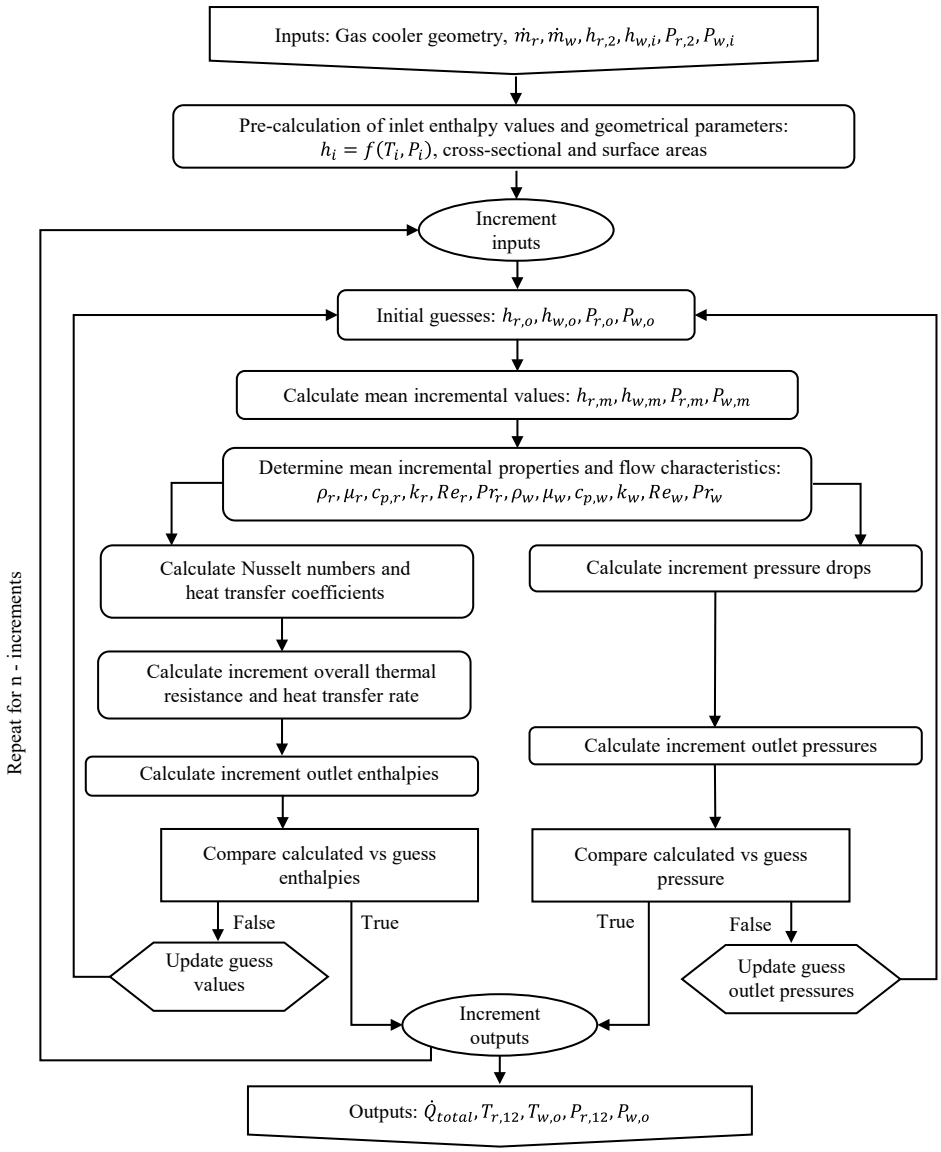

Figure 3: Gas cooler modelling flow diagram.

For R744 the Nusselt number is approached as a constant for laminar flow and correlated by Dittus-Boelter for turbulent flow (Cengel & Boles, 2015). Van Eldik *et al.* (2014) concluded this to be the most accurate approach when working with larger diameter tubes.

$$Nu = \begin{cases} 4.36 & (for\ laminar\ flow: Re < 2300) \\ 0.023 Re^{0.8}\,\mathrm{Pr}^{0.3} & (for\ turbulent\ flow: Re > 2300) \end{cases} \quad (1)$$

The waterside Nusselt number is determined from (Gnielinski, 1976):

$$Nu_w = \frac{\left(\frac{f_{fil}}{8}\right)(Re - 1000)Pr}{1 + 12.7\left(\frac{f_{fil}}{8}\right)^{0.5}(Pr^{\frac{2}{3}} - 1)} \quad (2)$$

Where f_{fil} is given by Dang and Hihara (2004):

$$f_{fil} = [1{,}82\log(Re) - 1.64]^{-2} \quad (3)$$

Accounting for only frictional pressure losses, the pressure drop can be calculated with the friction factor determined from Equation (3) for the refrigerant side, and the Darcy-Weisbach for the water (Cengel & Boles, 2015). The gas cooler model was verified against experimental results of van Eldik *et al.* (2014) with a maximum deviation of 5.3% for the predicted total heat transfer, with an average deviation of 2.9%.

2.2 Evaporator

The evaporator has a configuration where the R744 flows inside the tubes with air in cross flow over the finned outer surface, as shown in Figure 4. When assuming that the incoming refrigerant and air flow rates are uniformly distributed over the number of circuits, only a single circuit of the finned-tube evaporator needs to be modelled in detail. The R744 flows from the back of the circuit to the front in a counterflow configuration with respect to the airflow direction for improved heat transfer. Like the gas cooler, the circuit is divided into equal-length increments along the R744 flow direction, with the details of an increment shown in Figure 5. The heat exchanger has a staggered tube configuration with the front row tubes' air at the ambient condition, with the back row tubes' air an average of outlet conditions from the front row.

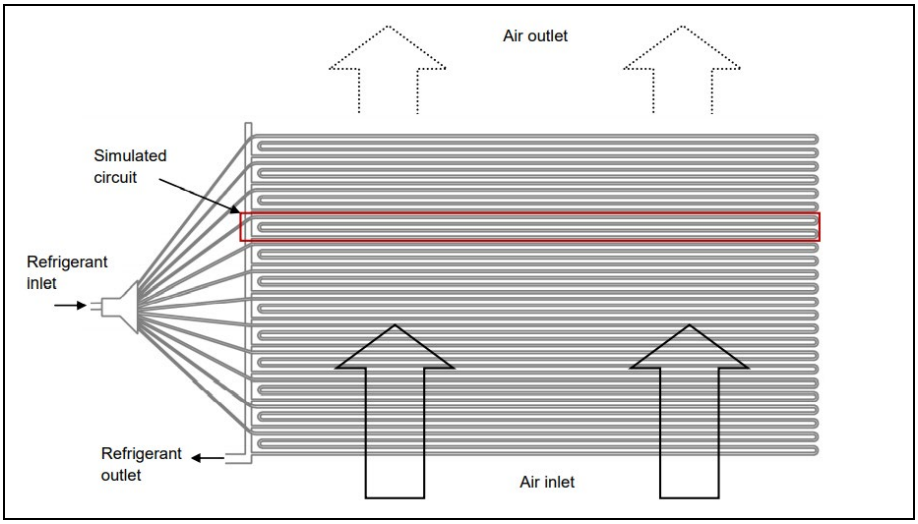

Figure 4: Frontal view of the finned-coil evaporator.

Geometrical inputs to the model include the materials of both the tubes and fins, tube diameters, total length of a single circuit, number of circuits, the fin thickness and pitch, tube pitch, and surface area ratios. The boundary conditions used include the expansion valve outlet enthalpy and pressure, moist air inlet temperature, pressure and relative humidity, and the mass flow rate of both fluids. To simplify the air side modelling, an assumption is made that an increment outer surface is either completely dry or wet. The flow diagram in Figure 6 represents the evaporator modelling approach followed, with the inlet and outlet states of the R744 corresponds with points (13) and (29) as denoted in Figure 1.

For two-phase flow boiling and pressure drop, the correlations by Cheng *et al.* (2008a&b) are used to evaluate the convective heat transfer coefficient and pressure drop. Their correlations are based on an empirical study where eight discrete flow patterns were identified. Wang *et al.* (2012, 2013) have concluded that only four of the eight flow

patterns' mass flux values are typically encountered in industrial R744 finned coil evaporators. The four flow patterns thus used in this study include intermittent, annular, dryout and mist. The reader is referred to the work by Cheng et al. (2008a&b) for the details of the equations used in modelling the four flow patterns, including the critical quality values that defines the transition between flow patterns. For the superheat region the Nusselt number is determined from Gnielinski (1976), given by Equation 2 above. The pressure drop within the superheated region is determined by using the Dang and Hihara (2004) friction factor, given by Equation 3.

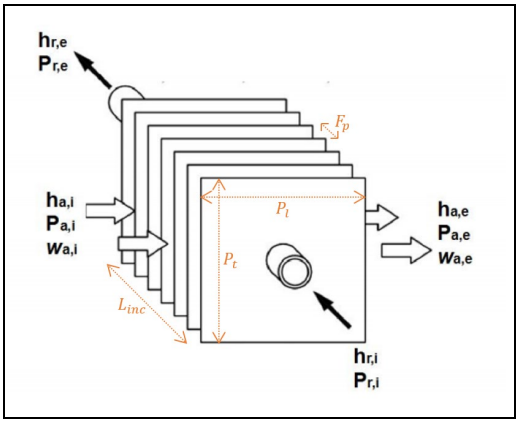

Figure 5: Details of an evaporator circuit increment.

For the air, both dry and wet conditions exist on the outer surface of the evaporator. For dry air the sensible heat transfer, $\dot{Q}_{a,s}$, between the bulk of the air stream and the outer tube wall can be equated from:

$$\dot{Q}_{a,s,dry} = h_{c,dry} A_{air,o} \eta_{o,dry} (T_a - T_{tw,o}) \tag{4}$$

where $T_{tw,o}$ represents the tube wall outer temperature. The dry air convection coefficient is calculated using Wang *et al.* (2000a). The sensible heat transfer for wet air, $\dot{Q}_{a,s,wet}$, is also calculated using Equation 4 for wet conditions. The wet air convection coefficient is calculated by Wang *et al.* (2000b). The latent heat transfer, $\dot{Q}_{a,l}$, is determined between the bulk of the air stream and the outer tube wall of the evaporator:

$$\dot{Q}_{a,l} = h_m A_{air,o} \eta_{o,wet} (\omega_w - \omega)(h_w - h_v) \tag{5}$$

with h_w, the condensate film enthalpy at the tube outer wall temperature, and ω_w the absolute humidity at the condensate film surface. The mass transfer coefficient, h_m, is correlated as a function of $h_{c,wet}$ (Pirompugd *et al.*, 2007). The frictional pressure drop for dry air is calculated by (Waltrich *et al.*, 2010):

$$\Delta P_{0L,dry} = \frac{\dot{m}_a^2}{2\rho_a A_{ff,a}} \left[\left(1 - \left(\frac{A_{ff,a}}{A_{frontal}} \right)^2 \right) \left(\frac{\rho_{a,i}}{\rho_{a,e}} - 1 \right) + 2 f_{a,dry} \frac{A_{air,o}}{A_{ff,a}} \left(\frac{\rho_{a,i}}{\rho_{a,i} + \rho_{a,e}} \right) \right] \tag{6}$$

where $f_{a,dry}$ is the dry friction factor (Wang *et al.*, 2000a). The frictional pressure loss for wet air, $\Delta P_{0L,wet}$, is calculated from Wang *et al.* (2002), which correlates the frictional loss under wet conditions as a function of the frictional loss under dry conditions. The evaporator model was verified against the work by Strydom (2013) with a maximum deviation of 6% for the predicted R744 temperature difference, and an average deviation of 2.5%. For the change in air temperature the maximum deviation was 5.7%, with an average deviation of 2.8%.

3. SYSTEM DESIGN SPECIFICATIONS

With this study mainly interested in the operations of the air-to-water heat pump cycle for higher ambient conditions combined with a high discharge water temperature, the specifications in Table 1 were used to select and design the main components.

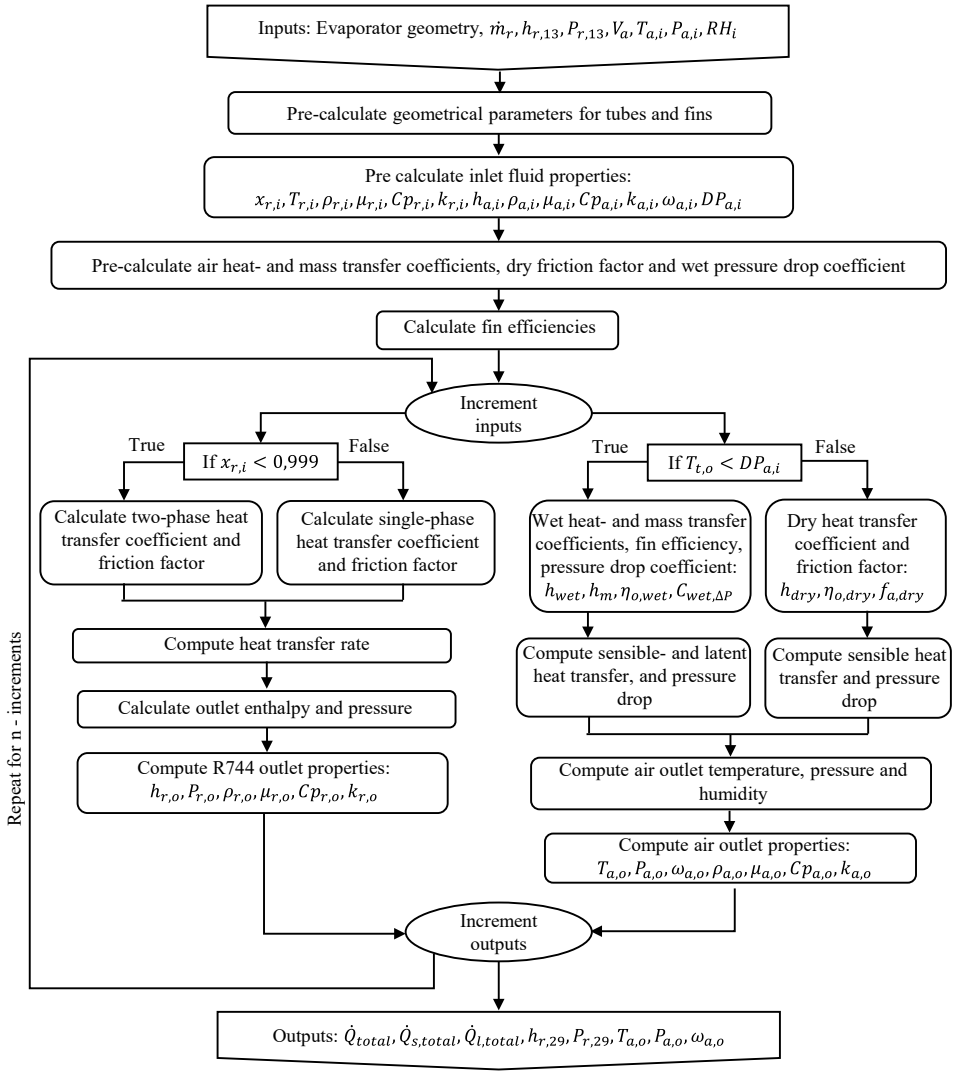

Figure 6: Evaporator modelling flow diagram

Table 1: Specifications for component design.

Fluid	Parameter	Symbol	Value	Unit
Water	Inlet temperature	$T_{w,i}$	15	[°C]
	Outlet temperature	$T_{w,o}$	90	[°C]
	Mass flow rate	$\dot{m}_w$	0.1	$[kg/s]$
Inlet air	Dry bulb temperature	$T_{a,i}$	25	[°C]
	Velocity	V_a	3.0	$[m/s]$
	Relative humidity	RH_i	30	[%]
	Pressure	$P_{a,i}$	85	$[kPa]$
R744	Evaporation	T_e	5.7	[°C]
	Degree of superheat	DOS	5	[°C]
	Discharge pressure	P_2	12	[MPa]

3.1 Compressor selection

From Table 1, the compressor must deliver a heating capacity of about 31.5kW for the conditions specified. The compressor selected for the design specifications is a semi-hermetic reciprocating type 4MTE-10K from Bitzer,

operated at 50 Hz. The method by Bester (2018) is used to develop a set of characteristic equations to model the R744 discharge temperature, T_2, as well as the mass flow rate, $\dot{m}$. The inputs to the compressor model include the suction pressure P_1 and temperature T_1, and discharge pressure P_2, with the coefficients given in Table 2. The compressor isentropic efficiency and work rate are then also calculated from this.

$$T_2 = \left[k_{1,1}(P_1) \cdot P_2 + k_{1,0}(P_1)\right] \cdot T_1 + \left[k_{0,1}(P_1) \cdot P_2 + k_{0,0}(P_1)\right] \quad (7)$$

$$\dot{m} = \left[k_{1,1}(P_1) \cdot P_2 + k_{1,0}(P_1)\right] \cdot T_1 + \left[k_{0,1}(P_1) \cdot P_2 + k_{0,0}(P_1)\right] \quad (8)$$

Table 2: Coefficients for the compressor characteristic equations.

Equation	Coefficient	Value
T_2	$k_{1,1}(P_1)$	$= (-1.9948e^{-2} \cdot P_1^3) + (3.0424e^{-1} \cdot P_1^2) + (-1.5261e^{0} \cdot P_1) + 2.5922e^{0}$
	$k_{1,0}(P_1)$	$= (2.3950e^{-1} \cdot P_1^3) + (-3.5242e^{0} \cdot P_1^2) + (1.7092e^{1} \cdot P_1) - 2.6687e^{1}$
	$k_{0,1}(P_1)$	$= (-4.4253e^{-1} \cdot P_1^2) + (2.5271e^{0} \cdot P_1) + 5.6828e^{0}$
	$k_{0,0}(P_1)$	$= (-2.7107e^{-0} \cdot P_1^3) + (4.3891e^{1} \cdot P_1^2) + (-2.4061e^{2} \cdot P_1) + 4.2585e^{2}$
$\dot{m}$	$k_{1,1}(P_1)$	$= (5.2808e^{-5} \cdot P_1^3) + (-7.4167e^{-4} \cdot P_1^2) + (3.5035e^{-3} \cdot P_1) - 5.5059e^{-3}$
	$k_{1,0}(P_1)$	$(-9.1276e^{-4} \cdot P_1^3) + (1.2011e^{-2} \cdot P_1^2) + (-5.3817e^{-2} \cdot P_1) + 7.9997e^{-2}$
	$k_{0,1}(P_1)$	$= (-7.0211e^{-4} \cdot P_1^3) + (9.1382e^{-3} \cdot P_1^2) + (-4.1873e^{-2} \cdot P_1) + 6.0374e^{-2}$
	$k_{0,0}(P_1)$	$= (3.9096e^{-2} \cdot P_1^2) + (-2.3501e^{-1} \cdot P_1) + 5.4477e^{-1}$

3.2 Heat exchanger specifications

For the conditions of Table 2, the designed counterflow gas cooler specifications are given in Table 3. The inner tube is made from AISI 304 Stainless Steel to handle the system pressure. Similarly, the designed aluminum finned, copper tube evaporator specifications are given in Table 4 for the required cooling capacity.

Table 3: Gas cooler specifications.

Symbol	Name	Value	Unit
$D_{i,i}$	Inner tube inside diameter	0.016	$[m]$
$D_{o,i}$	Outer tube inside diameter	0.026	$[m]$
t_{wall}	Inner tube wall thickness	0.00275	$[m]$
L_{gc}	Gas cooler tube length	28.06	$[m]$

Table 4: Evaporator specifications.

Symbol	Name	Value	Unit
σ	Ratio of free flow area over frontal area	0.534	$[-]$
α	Ratio of air surface area over volume	587	$[-]$
A_{fin}/A	Ratio of fin surface area over total air surface area	0.913	$[-]$
D_i	Inner tube diameter	0.00938	$[m]$
N_{tr}	Number of tube rows	2	$[-]$
F_p	Fin pitch	0.003175	$[m]$
P_t	Transversal tube pitch	0.0254	$[m]$
P_l	Longitudinal tube pitch	0.022	$[m]$
δ_f	Fin thickness	0.00033	$[m]$
L_{evap}	Tube length (for a single parallel circuit)	5.63	$[m]$
$N_{c,evap}$	Number of parallel circuits	12	$[-]$

4. RESULTS

Using the cycle simulation developed an investigation was done for fixed inlet and outlet water temperatures of 15°C and 90°C respectively, over a range of ambient temperature of 25°C to 40°C at 30% RH, to determine at which discharge pressure the best heating COP can be obtained. Figure 7 shows that at 25°C and 30°C ambient, the optimum discharge pressure (ODP) lies within the range of 12.5-13.0 MPa, whereas for 35°C and 40°C the ODP is in the 13.0-13.5 MPa range. As the ambient rose from 25°C to 40°C, the highest recorded COP value improved by 9.6% from 2.81 to 3.07. The increase in ODP for a rise in ambient temperature agrees with Wang *et al.* (2013).

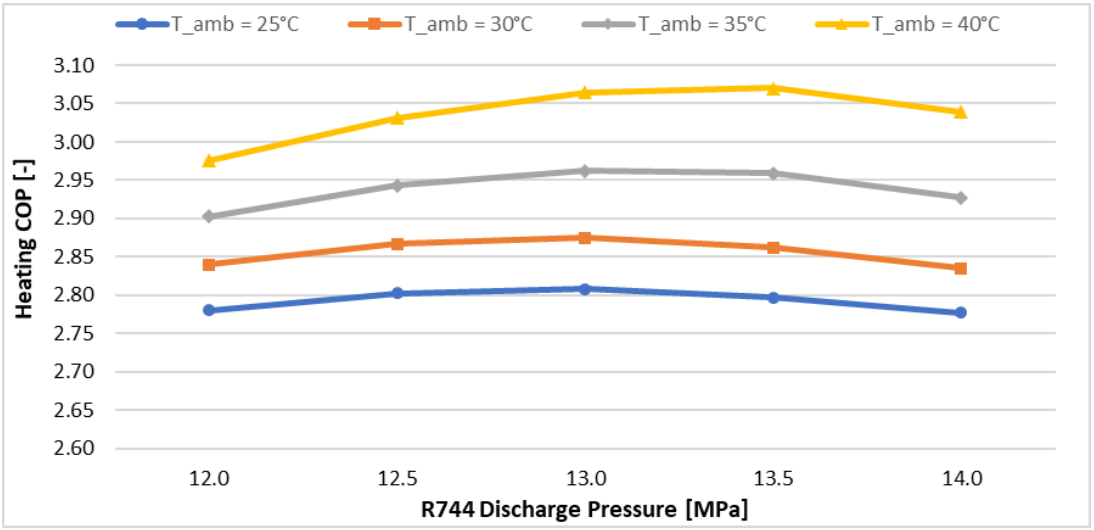

Figure 7: Heating COP for 90°C water discharge at various ambient conditions over a range of discharge pressures.

For any heating system the water is circulated through the heat pump until the storage vessel is at the required temperature. This means that the heat pump will experience increasing inlet water temperatures during an operating cycle. For an ambient temperature of 25°C with a 30% RH, and a water outlet temperature of 90°C, the cycle performance was evaluated at water inlet temperatures ranging from 15°C to 60°C. From Figure 8 it is evident that the heating COP substantially decrease with a rise in water inlet temperature. When the water inlet rose from 15°C to 60°C, the maximum cycle COP decreased from 2.81 to 1.87.

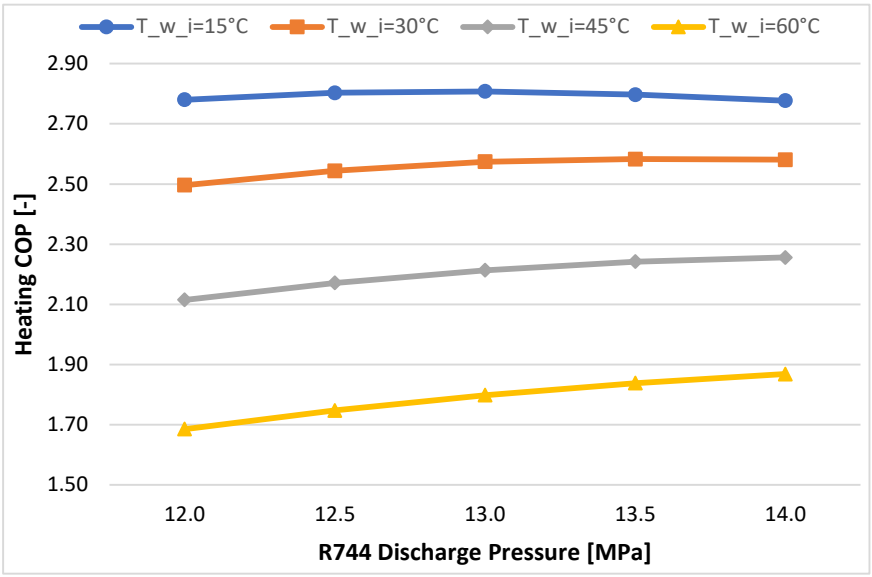

Figure 8: Heating COP at 90°C water discharge for varying inlet temperatures over a range of discharge pressures.

5. CONCLUSIONS

This paper described the cycle simulation, including the detailed component modelling, specifically developed to investigate the use of R744 heat pumps for application in industrial process heat, when operated in South African ambient conditions. The model was developed to determine system performance in warm ambient conditions between 25°C and 40°C, while heating water to 90°C as required for industrial processes. Preliminary results showed a correlation with literature when evaluating the operations of such a cycle. With the heat pump cycle model now developed, a more detailed study will follow that will focus on the use of R744 heat pumps for industrial processes and specifically the operating envelope of the technology over a wide range of operating conditions. This planned study aims to manufacture of a fully instrumented prototype high temperature heat pump for installation within an industrial process for comparison against the detailed modelling results. The seasonal effect on the performance of the technology for high discharge temperatures can then be analyzed in more detail. If the technology can be successfully implemented, it will result in the South African industrial sector becoming more energy efficient and less dependent on coal. This is not only applicable to South Africa as a country, but an opportunity for the industrial sector in Africa to become more energy efficient.

NOMENCLATURE

A	area	(m^2)
COP	coefficient of performance	(–)
D	diameter	(m)
D_h	hydraulic diameter	(m)
DOS	degree of superheat	(°C)
DP	dew point	(°C)
η	efficiency	(–)
f	friction factor	(–)
h	enthalpy	(J/kg)
h_c	convection coefficient	(W/m^2K)
h_m	mass transfer coefficient	(kg/m^2s)
k	thermal conductivity	(W/mK)
L	length	(m)
$\dot{m}$	mass flow	(kg/s)
Nu	Nusselt number	(–)
P	pressure	(Pa)
Pr	Prandtl number	(–)
$\dot{Q}$	heat transfer	(W)
Re	Reynolds number	(–)
RH	relative humidity	(%)
ρ	density	(kg/m^3)
T	temperature	(°C)
V	velocity	(m/s)
ω	humidity ratio	(kg_w/kg_a)

Subscript

a	air
amb	ambient
dry	dry
e	evaporation
ff	free flow
frontal	frontal area
i	inlet, inner
l	latent
o	outlet, outer
r	refrigerant

s	sensible
tw	tube wall
v	vapour
w	water
wet	wet

REFERENCES

1. Bester, J., 2018. *A methodology for the performance characterisation of a variable speed CO2 compressor,* Potchefstroom: North-West University.
2. Cao, F., Ye, Z. & Wang, Y., 2020. Experimental investigation on the influence of internal heat exchanger in a transcritical CO2 heat pump water heater. *Applied Thermal Engineering,* Volume 168, pp. 1-11.
3. Cengel, Y. & Boles, M., 2015. *Thermodynamics: An Engineering Approach.* 8th ed. New York: McGraw-Hill Education.
4. Cheng, L., Ribatski, G., Quiben, J. & Thome, J., 2008a. New prediction methods for CO2 evaporation inside tubes: Part I - a two-phase flow pattern map and a flow pattern based phenomenological model for two-phase flow frictional pressure drops. *International Journal of Heat and Mass Transfer,* Volume 51, pp. 111-124.
5. Cheng, L., Ribatski, G. & Thome, J., 2008b. New prediction methods for CO2 evaporation inside tubes: Part II - An updated general flow boiling heat transfer model based on flow patterns. *International Journal of Heat and Mass Transfer,* Volume 51, pp. 125-135.
6. Dang, C. & Hihara, E., 2004. In-tube cooling heat transfer of supercritical carbon dioxide. Part 2. Comparison of numerical calculation with different turbulence models. *International Journal of Refrigeration,* Volume 27, pp. 748-760.
7. Gnielinski, V., 1976. New evaluation for heat and mass transfer in turbulent pipe and channel flow. *International Jounral of Chemical Engineering,* Volume 16, pp. 359-368.
8. IEA (2021), World Energy Outlook 2021, IEA, Paris, https://www.iea.org/reports/world-energy-outlook-2021.
9. Kim, S., Kim, Y., Lee, G. & Kim, M., 2005. The performance of a transcritical CO2 cycle with an internal heat exchanger for hot water heating. *International Journal of Refrigeration,* Volume 28, pp. 1064-1072.
10. Pirompugd, W., Wang, C. & Wongwises, S., 2007. Finite circular fin method for heat and mass transfer characteristics for plain fin-and-tube heat exchangers under fully and partially wet surface conditions. *International Journal of Heat and Mass Transfer,* Volume 50, pp. 552-565.
11. Strydom, 2013. *Thermal-fluid simulation of an air-to-CO2 finned coil evaporator,* Potchefstroom: North-West University.
12. Van Eldik M, Harris PM, Kaiser WH, Rousseau PG, "Theoretical and experimental analysis of supercritical carbon dioxide cooling", 15th International Refrigeration and Air Conditioning Conference at Purdue, July 14-17, 2014.
13. Waltrich, M., Hermes, C., Goncalves, J. & Melo, C., 2010. A first-principles simulation model for the thermo-hydraulic performance of fan supplied tube-fin heat exchangers. *Applied Thermal Engineering,* 30(14), pp. 2011-2018.
14. Wang, C., Chi, K. & Chang, C., 2000a. Heat transfer and friction characteristics of plain fin-and-tube heat exchangers, part II: Correlation. *International Journal of Heat and Mass Transfer,* 43(2000), pp. 2693-2700.
15. Wang, C., Lin, Y. & Lee, C., 2000b. An airside correlation for plain fin-and-tube heat exchanger in wet conditions. *International Journal of Heat and Mass Transfer,* 43(2000), pp. 1869-1872.
16. Wang, C., Lee, W. & Sheu, W., 2002. A New Approach to Correlate the Frictional Performance of Fin-and-Tube Heat Exchaners in Wet Conditions. *Heat Transfer Engineering,* Volume 23, pp. 15-21.
17. Wang, C., Hafner, A., Kui, C. & Hsieh, W., 2012. An overview of the effect of lubricant on the heat transfer performance on conventional refrigerants and natural refrigerant R-744.. *Renewable and Sustainable Energy Reviews,* 16(7), pp. 5071-5086.
18. Wang, S., Tuo, H., Cao, F. & Xing, Z., 2013. Experimental investigation on air-source transcritical CO2 heat pump water heater system at a fixed water inlet temperature. *International Journal Of Refrigeration,* Volume 36, pp. 701-716.
19. Yamaguchi, S., Kato, D., Saito, K. & Kawai, S., 2011. Development and validation of static simulation model for CO2 heat pump. *International Jounral of Heat and Mass Transfer,* Issue 54, pp. 1896-1906.
20. Ye, Z. et al., 2020. Optimal discharge pressure in transcritical CO2 heat pump water heater with internal heat exchanger based on pinch point analysis. *International Journal of Refrigeration,* Volume 118, pp. 12-20.